Asian Journal of Chemistry; Vol. 38, No. 6 (2026), 1629-1640
ASIAN JOURNAL OF CHEMISTRY
https://doi.org/10.14233/ajchem.2026.36010

Spectroscopic Structural Elucidation and Molecular Docking Studies of Newly Isolated Rhamnose Containing Hexaoligosaccharide from Mango Honey: Implications for Wound Healing Activity

AKANKSHA YADAV[1], APARNA SHARMA[1], RANVIJAY PRATAP SINGH[2] and SHASHI BALA[1,*]

[1]Department of Chemistry, University of Lucknow, Lucknow-226007, India
[2]Department of Applied Science & Humanities, Faculty of Engineering and Technology, University of Lucknow, Lucknow-226031, India

*Corresponding author: E-mail: shashichem15@gmail.com

Received: 16 March 2026 *Accepted*: 21 May 2026 *Published online*: 31 May 2026 AJC-22390

A novel rhamnose-containing oligosaccharide, magnorhamnose ($C_{41}H_{72}N_2O_{30}$), was isolated from the chloroform extract of mango honey using silica gel column chromatography with chloroform and methanol as the mobile phase. The honey sample was extracted using a modified method involving acetylation followed by chloroform extraction, which facilitated the isolation of the oligosaccharide fraction. The isolated compound showed positive results in the phenol-sulphuric acid, Feigl and Morgan-Elson tests, confirming the presence of carbohydrate moieties along with *N*-acetyl-containing monosaccharide units. Based on these structural characteristics, PASS analysis was performed to predict its potential biological activities. The compound exhibited promising antimicrobial and antifungal activities with Pa values of 0.751 and 0.740, respectively, indicating its possible therapeutic relevance. To further support these predictions, molecular docking studies were carried out against five proteins associated with wound-healing activity, namely 1FLT, 1Q7D, 2AZ5, 6Y8M, and 6B8Y. Magnorhamnose demonstrated favorable binding affinities with docking energies of -8.0, -5.2, -7., -5.6 and -5.6 kcal/mol, respectively. The combined findings from phytochemical characterization, PASS prediction, and molecular docking analysis suggest that magnorhamnose possesses potential antimicrobial and wound-healing properties, warranting further experimental investigation.

Keywords: Honey, Rhamnose, Hexa-saccharide, 2D-NMR spectrometry, Wound healing.

INTRODUCTION

Since ancient times, honey has been widely used in Ayurvedic and Unani systems of medicine due to its numerous therapeutic properties. The medicinal value of honey depends not only on the floral source from which it is derived, but also on factors such as storage conditions, duration of storage, and its combination with other natural extracts. Previous studies have shown that honey is primarily a carbohydrate-rich natural syrup containing sugars such as fructose, glucose, rhamnose, maltose, furanose, maltotriose and panose [1,2]. In addition, raffinose and melezitose have also been reported in nectar by several researchers. Owing to its diverse chemical composition, honey exhibits a broad range of biological activities including antifungal, antibacterial, cytostatic and antitumor properties. Furthermore, honey and honey-derived products have been extensively recognized for their wound-healing and anti-inflammatory effects, making them valuable in the traditional as well as modern therapeutic applications [3].

Besides this, honey showed the immune-modulatory effects of which enhance wound healing and various ingredients like phenolic compounds, flavonoids and their glycosides, present in honey, contributed for anti-inflammatory and antioxidant properties of honey [4]. In honey, more than 200 different compounds were reported, such as sugar, minerals, organic acids, enzymes, proteins, vitamins and polyphenolic compounds [5]. Manuka honey is widely used as a wound dressing agent due to its well-established therapeutic and antimicrobial properties [6]. In contrast, honey derived from *Camellia oleifera* has been reported to possess cardioprotective effects, including the prevention of hypertension, coronary heart disease, and atherosclerosis [7]. These beneficial effects are attributed to its easy digestion and rapid absorption in the human body, which may contribute to the reduction of blood pressure and blood lipid levels as well as improvement in blood vessel elasticity [8]. Another constituent of honey, *i.e.*, quercetin, shows benefits overall health and disease resistance including antiviral, anti-carcinogenic, antioxidant, anti-carcinogen and psy-

chostimulant activity [9]. The HPLC profile of ingredients of *Robinia pseudoacacia* nectar had shown the presence of rhamnose into its glycosides [10].

Review articles of Khachemoune *et al.* [11,12] focused on raising awareness about the potential applications of honey in various wound treatments, which has nowadays become a rapidly growing area of research. Previous studies have reported that Saudi Tamarix honey (STH) contains flavonoids with significant wound-healing potential. Molecular docking investigations demonstrated a high probability score (0.52-1.0) against two wound healing-related targets, GSK-3β and NOX4, suggesting strong target affinity and possible therapeutic relevance in wound management [13]. Considering the wide range of medicinal properties associated with honey, mango honey (600 g) was collected for the isolation and characterization of bioactive oligosaccharides. The honey sample was subjected to a modified extraction procedure involving *in situ* acetylation using acetic anhydride and pyridine. The reaction mixture was concentrated under reduced pressure and subsequently partitioned between water and chloroform. The resulting chloroform extract was purified by silica gel column chromatography, leading to the isolation of a rare hexasaccharide, designated as magnorhamnose.

The structural investigation revealed that magnorhamnose is composed of rhamnose, mannose, ManNHAc, glucose and GlcNHAc units. The uniqueness of this compound lies in the presence of rhamnose as the terminal reducing monosaccharide within a long-chain oligosaccharide structure. To the best of current knowledge, this is the first report of a naturally occurring oligosaccharide containing rhamnose in such a configuration isolated from a natural source. Earlier studies on honey oligosaccharides mainly reported fructose-, glucose- and galactose-based saccharides, whereas the occurrence of rhamnose as a terminal reducing sugar has not previously been documented. The modified extraction methodology may have contributed to the successful isolation of this long-chain oligosaccharide from honey. To evaluate its possible biological significance, magnorhamnose was also subjected to PASS analysis, which provided preliminary evidence for potential bioactivity and supported further computational and experimental investigations. In addition, molecular docking studies were performed against five proteins associated with wound-healing pathways, namely 1FLT, 1Q7D, 2AZ5, 6Y8M and 6B8Y.

EXPERIMENTAL

Sugars were visualized on TLC plates using 50% aqueous H_2SO_4 as the spraying reagent. Silica gel G was used as the adsorbent for thin-layer chromatography, while silica gel (SRL, 60–120 mesh) was employed for column chromatography. Authentic standards of glucose, mannose, mannosamine, and rhamnose were obtained from Sigma-Aldrich and used for comparative identification studies.

Structural elucidation of the isolated oligosaccharide was performed using 1D and 2D NMR spectroscopy. The acetylated oligosaccharide was analyzed in $CDCl_3$, whereas the natural oligosaccharide was recorded in D_2O at 25 ºC on a Bruker AM spectrometer operating at 300 MHz for ^1H NMR and 75 MHz for ^{13}C NMR analysis. For mass spectrometric characterization, the sample was dissolved in suitable solvents such as methanol, acetonitrile or water and introduced into the electrospray ionization (ESI) source through a syringe pump at a flow rate of 5 μL/min. The ESI capillary voltage was maintained at 3.5 kV, while the cone voltage was set at 40 V.

Isolation of honey oligosaccharide: The honey sample (40 g), collected from a mango orchard in the Gonda district of Uttar Pradesh, India, was concentrated under reduced pressure. The obtained residue (20 g) was further lyophilized to dryness, yielding a brown-coloured dry powder (10 g). The powdered sample (8 g) was then acetylated using acetic anhydride (8 mL) and pyridine (8 mL). The reaction mixture was heated for 1 h followed by overnight stirring to ensure complete acetylation of the oligosaccharide constituents. After completion of the reaction, the mixture was concentrated under reduced pressure until a dry powder was obtained. The resulting material was partitioned between water and chloroform. The chloroform fraction was subsequently washed with water and dried over anhydrous sodium sulphate. Removal of the solvent under reduced pressure afforded 8.5 g of an acetylated oligosaccharide mixture. TLC analysis of the acetylated mixture using $CHCl_3$:MeOH (95:5) as the mobile phase revealed five distinct spots. The acetylated oligosaccharide mixture was further purified by silica gel column chromatography for the isolation of individual compounds.

Silica column chromatography of acetylated mixture of oligosaccharide: The acetylated oligosaccharide mixture (8 g) was subjected to silica gel column chromatography using 400 g of silica gel as the stationary phase. Elution was carried out using chloroform followed by $CHCl_3$:MeOH mixtures of varying proportions, and fractions of 200 mL were collected throughout the separation process. Fractions showing similar TLC profiles were pooled together, resulting in the isolation of a pure novel oligosaccharide acetate, designated as magnorhamnose acetate (88 mg).

Deacetylation of magnorhamnose acetate: Isolated magnorhamnose acetate (35 mg) was dissolved in acetone (3.5 mL), followed by the addition of NH_3 solution (3.5 mL). The reaction mixture was kept in a stoppered flask in the dark for 24 h to facilitate deacetylation. After completion of the reaction, the mixture was concentrated to dryness under reduced pressure. To remove the acetate groups in the form of acetamide, the resulting residue was partitioned between water and $CHCl_3$ (2 × 2.5 mL). The aqueous layer was separated and subsequently lyophilized to yield the natural deacetylated oligosaccharide, designated as compound C (28 mg). The isolated compound, magnorhamnose ($C_{41}H_{72}N_2O_{30}$, *m.w.* 1073), was dried over P_2O_5 at 100 ºC for 8 h to remove residual moisture. The purified compound gave positive results in the phenol-sulphuric acid [14], Feigl [15] and Morgan-Elson tests [14], confirming its oligosaccharide nature and indicating the presence of *N*-acetyl-containing monosaccharide residues within the structure.

^1H NMR ($CDCl_3$, 300 MHz, δ ppm): 6.35 (α-(S-1)), 6.25 (β-rhamnose (S-1)), 5.50 (d, H-3, α-ManNHAc (S-2)), 4.90 (d, H-2, β-glucose (S-3) of (S-1)), 5.20 (d, H-3, β-mannose (S-4)), 5.60 (d, H-2, α-Glc (S-5)), 5.70 (d, H-2, β-manNHAc (S-6)); ^1H NMR (D_2O, 300 MHz, δ ppm): 1.77 (3H, S-2),

1.99 (H-2 of S-6); ^{13}C NMR ($CDCl_3$, 75 MHz, δ ppm): 90.00 (α-S-1), 92.00, rhamnose (S-1) C-1), 90.80, α-ManNHAc (S-2) C-3 (S-1)), 95.29 (β-Glc (S-3) C-4 of (S-1), 92.00 (β-mannose (S-3) C-4), 93.59 (α-Glc (S-5) C-2), 91.61 (S-6) C-2). Mass spectrum: *m/z* 1073 (M^+), 1091 ($M^+ + NH_4^+ + CO_2$), 1057 ($M^+ + NH_4^+$), 949 ($M^+ + Na^+$), 162 ($C_6H_{12}O_6$-H_2O), 187 ($C_6H_{12}O_6 + 7H^+$).

Preparation of protein and ligand for docking: High-resolution crystal structures of IL-1β (PDB ID: 6Y8M), TNF-α (PDB ID: 2AZ5), VEGF (PDB ID: 1FLT), collagen α-1 (PDB ID: 1Q7D) and TGF-β receptor I kinase (PDB ID: 6B8Y) were retrieved from the Protein Data Bank. The protein structure was prepared for molecular docking studies using AutoDock tools (ADT) version 1.5.7, developed by the molecular graphics laboratory [16]. During receptor preparation, heteroatoms, water molecules and any co-crystallised ligands were removed from the PDB structure. Polar hydrogen atoms were added and Kollman united atom charges were assigned. The prepared receptor structure was then saved in the PDBQT format for docking analysis [17]. For ligand preparation, compound was geometrically optimised using the B3LYP functional with the 6-31G(d,p) basis set in the Gaussian 09 program package. The optimised structure was saved in .mol2 format. Subsequently, PyMOL (version 2.4.1.0) was used to convert the .mol2 files into PDB format. Finally, the ligand structures were imported into AutoDock Tools and saved in PDBQT format for docking studies.

Docking studies: All molecular docking simulations were performed using AutoDock vina [18]. The docking results and intermolecular interactions between the receptor and ligand molecules were analysed using BIOVIA Discovery Studio (Dassault Systèmes BIOVIA, San Diego, USA) and PyMOL [19]. For each ligand, the binding conformation with the highest binding affinity (lowest Vina score) and the lowest root mean square deviation (RMSD) were selected for further analysis. The electrostatic grid box for docking was defined with a grid spacing of 0.375 Å. The grid box center 1FLT (set at X = 0.375 Å, Y = -2.631 Å and Z = 20.344 Å), 1Q7D (set at X = 4.507 Å, Y = 32.622 Å and Z = 0.568 Å),2AZ5 (set at X = -14.039 Å, Y = 71.422 Å and Z = 27.435 Å), 6Y8M (set at X = 15.865 Å, Y = 13.280 Å and Z = -9.205 Å) and 6B8Y (set at X = 9.020 Å, Y = 1.082 Å and Z = 12.251 Å), with dimensions of 40 × 40 × 40 Å along the X, Y and Z axes, respectively.

RESULTS AND DISCUSSION

Structure elucidation of compound C (magnorhamnose): Magnorhamnose gave positive tests in Fiegl, phenol-sulphuric acid and Morgan-Elson test, confirming it to be a reducing sugar with the presence of *N*-content into its constituent monosaccharides. It was isolated into its acetylated form and abbreviated as 'c' whiles its natural oligosaccharide as 'C'. The name of the compound magnorhamnose, was extracted from the source of honey *i.e. M. indica* (Mango).

The ^{1}H NMR spectrum of magnorhamnose acetate displayed several characteristic anomeric proton signals, indicating the presence of multiple sugar residues within the oligosaccharide framework (Fig. 1a). These proton resonances were further supported by the corresponding ^{13}C NMR signals

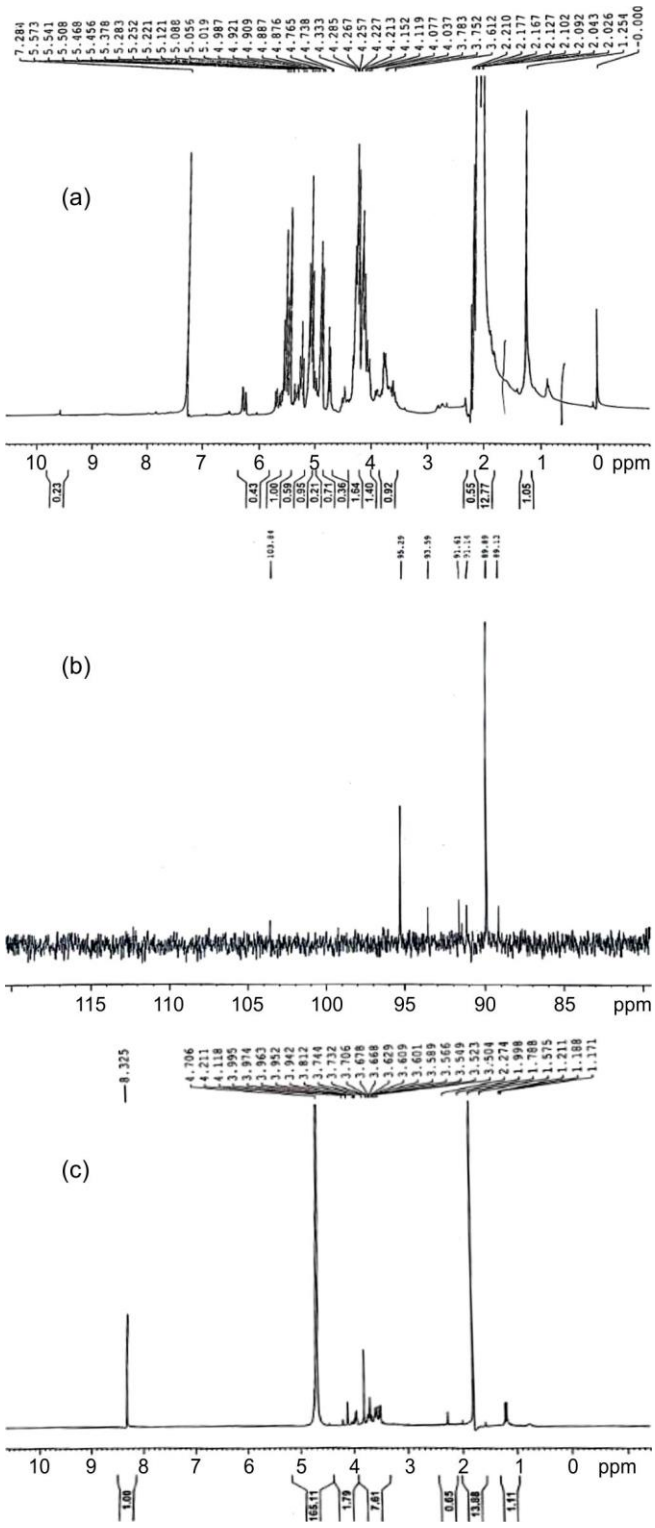

Fig. 1. ^{1}H NMR of magnorhamnose acetate in (a) $CDCl_3$ at 300 MHz, (b) $CDCl_3$ at 75 MHz and (c) D_2O at 300 MHz

observed in the anomeric carbon region (Fig. 1b). The combined proton and carbon spectral data confirmed that magnorhamnose acetate is composed of six monosaccharide units linked together in a hexasaccharide structure. The observed coupling patterns and chemical shift distribution further suggested the presence of both α- and β-configured sugar moieties within the molecule, supporting the structural complexity of

the isolated oligosaccharide. Furthermore, the structural confirmation obtained from the ^{1}H NMR spectrum of the purified deacetylated oligosaccharide (magnorhamnose), displayed two characteristic signals at δ 1.78 and δ 1.99 (Fig. 1c). These peaks are indicative of two *N*-acetyl groups present within the oligosaccharide structure, supporting the occurrence of *N*-acetylated monosaccharide residues in the compound.

The HSQC spectrum of magnorhamnose acetate contain seven cross peaks at δ 90.0×6.35 (α-S1), δ 92.0×6.25 (β-S1), δ 90.80×5.50 (S2), δ 95.29×4.90 (S3), δ 92.0×5.20 (S4), δ 93.59×5.60 (S5) and δ 91.61×5.7 (S6) confirming the presence of six monosaccharides in compound C in its reducing form (Fig. 2).

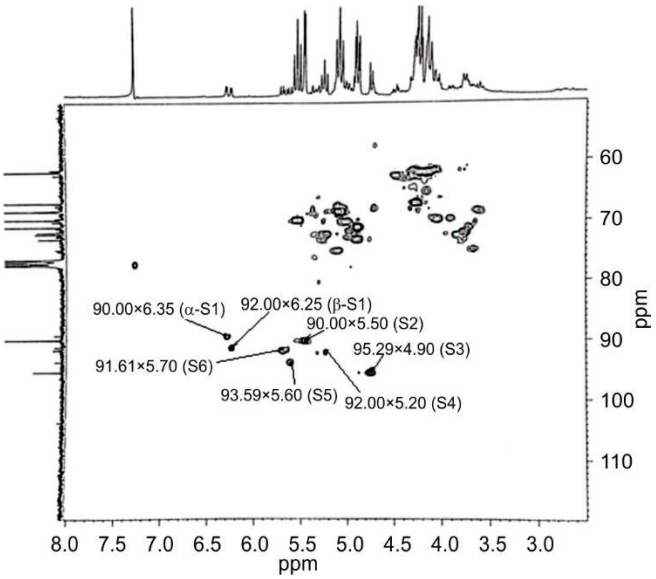

Fig. 2. HSQC spectrum of magnorhamnose acetate in $CDCl_3$ at 300 MHz

The splitting pattern of anomeric proton at δ 6.25 (J = 3.6 Hz) along with the ^{13}C NMR chemical shift value of reducing monosaccharides at δ 92.0 resembles with the literature value of β-L-Rha*p* in their $^1C_4$ conformation [20,21]. It was also confirmed by authentic sample analysis. While α-value of S1 gave their cross peaks at δ 90.00 × 6.35. These results were in conformity with the results obtained from methylglycosidation/acid hydrolysis of magnorhamnose acetate [22,23]. The compound magnorhamnose acetate undergoes for Killiani hydrolysis [21,23] confirmed the presence of L-Rha*p*, D-Glc*p*, D-Man*p*, D-Man*p*NAc (**Scheme-I**), which confirmed by TLC and NMR spectra with authentic sample.

Further, it confirms the chain elongation in the oligosaccharide '**C**', by the TOCSY and COSY spectrum of magnorhamnose acetate was analysed. In HSQC spectrum the ring protons of S1, which gave cross peaks at δ 6.25×92.00. TOCSY spectrum shown, three cross peaks each δ 6.25×3.98, δ 6.25 ×4.10 and δ 6.25×5.28, respectively. The results, obtained from TOCSY spectrum further reviewed by COSY spectrum that the ring protons of S1were confirmed as δ 3.98 (H-2), δ 4.1(H-3) and δ 5.28 (H-4), respectively. Presence of methyl group in Rha*p* was also confirmed by the presence of ^{1}H NMR value at δ 1.25 in ring S1 and cross confirmed by authentic sample of Rha*p*. The confirmation of reducing monosaccharide was done by reduction and rhamnose converted into rhamnitol [24]. In ring S1, one value at δ 3.98 may be considered for chain elongation in hexa-saccharide. Since, the position of δ 3.98 does not give any cross peak in HMBC spectrum, instead, it gave a cross peak in COSY spectrum of magnorhamnose acetate showed two values at δ 3.98 and δ 4.10 for H-2 of S3 and H-3 of S2 for glycosidic linkage by the next monosaccharide (Fig. 3).

Hence, absences of any cross peaks in HMBC spectrum, hindering the linkage process of the oligosaccharides. To overcome this problem, the chemical shift value at δ 3.98 was observed in HSQC spectrum, which gave a cross peak at δ 3.98×70.00, which was again observed in HMBC spectrum that gave a cross peak between δ 70.00×4.90 (reverse HMBC)

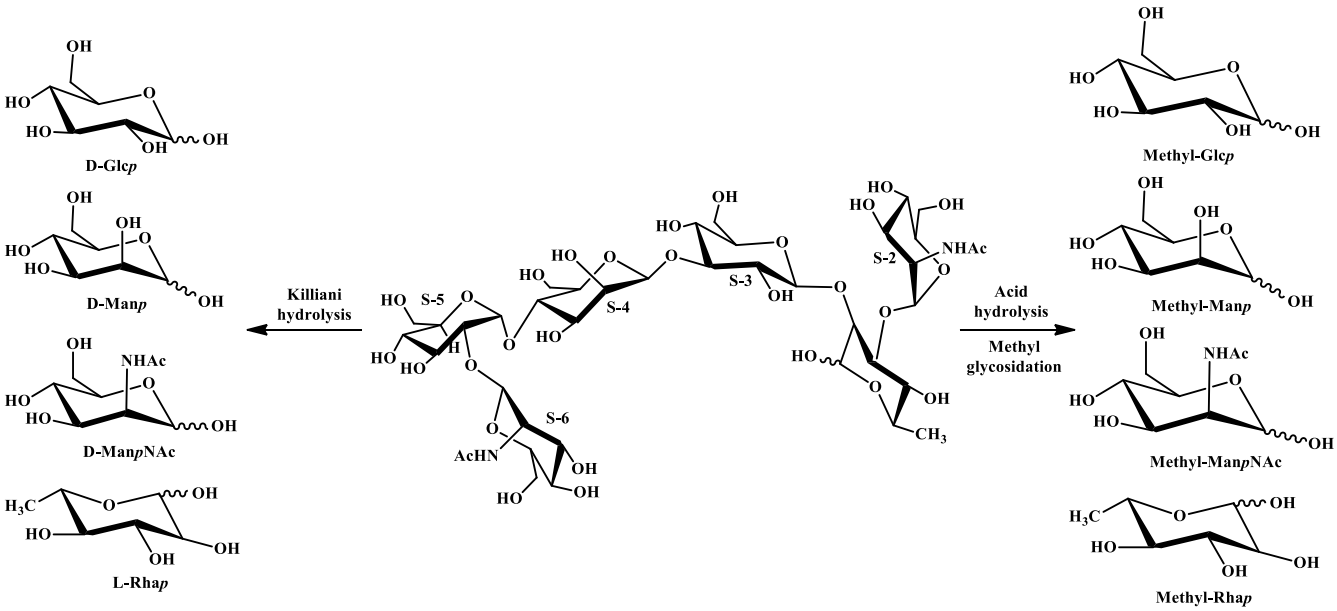

Scheme-I: Killiani hydrolysis and methylglycosidation/acid hydrolysis of magnorhamnose

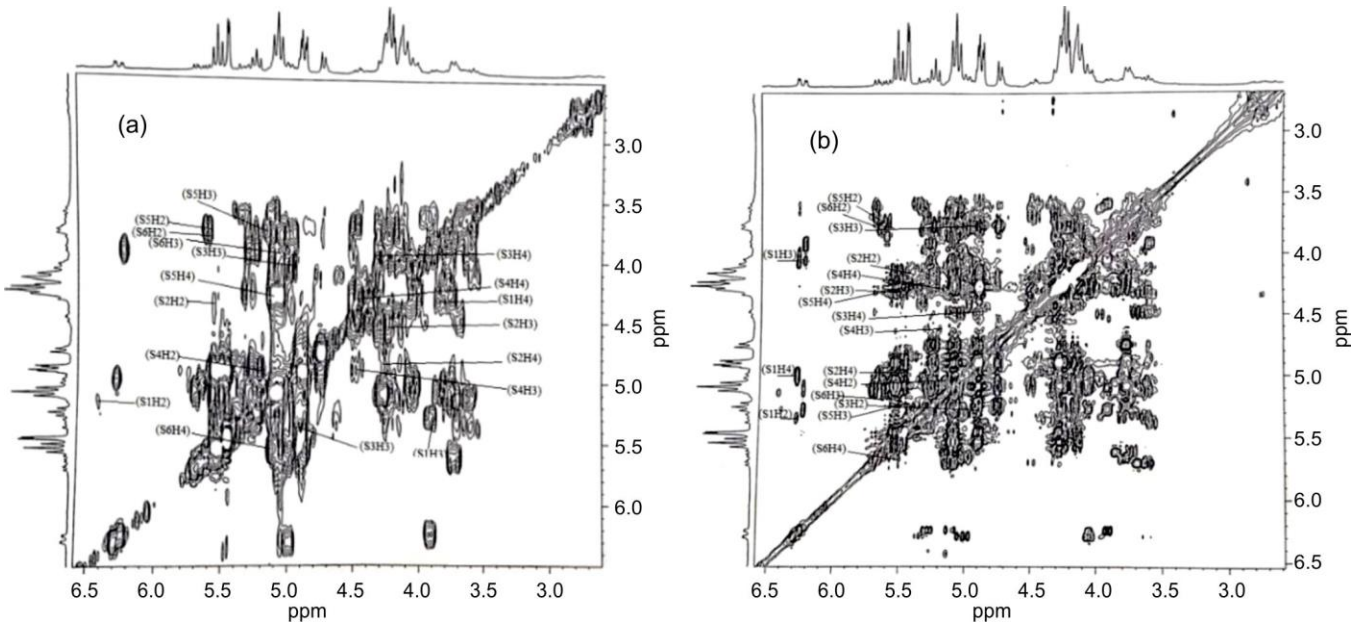

Fig. 3. (a) TOCSY and (b) COSY spectra of magnorhamnose acetate in $CDCl_3$ at 300 MHz

[25] confirming (1→2) linkage between S1 and S3. Not only H-2 of S1 gave linkage opportunity with another oligosaccharide, but H-3 of S1 also can link with next monosaccharides. This value is δ 4.1 (H-3) also confirmed the connectivity by reverse HMBC process between S1 and S2 (Fig. 4).

The anomeric proton value of S2 at δ 5.50 gave three cross peaks at δ 5.5×4.11, δ 5.5×4.28 and δ 5.5×4.86 confirmed that none of its hydroxyl group was involved in glycosidic linkage and hence S2 was at non-reducing end of magnorhamnose acetate [26]. Hence S2 was confirmed as Man*p*NAc the ring proton present at δ 4.1, reflected for the presence of NAc group in H-2 of S2, which also confirmed by ^{1}H NMR spectrum of magnorhamnose in D_2O solvent for which *J* value was 3.6 Hz. Further the ring proton present at δ 5.50 (*J* = 3.6 Hz) confirmed a α-glycosidic linkage between S2 and S1 and $^4C_1$ L confirmation for sugar S-2. Though, there was two positions were available in S1 *i.e.*, position H-2 and H-3 for glycosidic linkage by the monosaccharide unit. Further, the value of H-2 at δ 3.98, was observed in HMBC spectrum which did not show any cross peak in HMBC spectrum hence it was again observed in HSQC spectrum which gave a cross peak at δ 70.00. This value further gave a cross peak at δ 70.00×4.90 confirming a (1→2) linkage between S3 and S1 (reverse HMBC) [25]. The anomeric proton value of δ 4.90 gave a cross peak at δ 95.29 in the HSQC spectrum of magnorhamnose acetate confirming anomeric proton/carbon value of S3 as δ 4.90 and δ 95.29. These values resemble with the literature value of Glucose and hence S3 was confirmed as Glc [27,28]. The *J* value of anomeric proton at δ 4.90 (*J* = 6.6 Hz) confirmed the β-glycosidic linkage between S3 and S1 and $^4C_1$ D conformation for S-3. Further, the TOCSY spectrum of S3 with anomeric proton signal δ 4.90 gave three cross

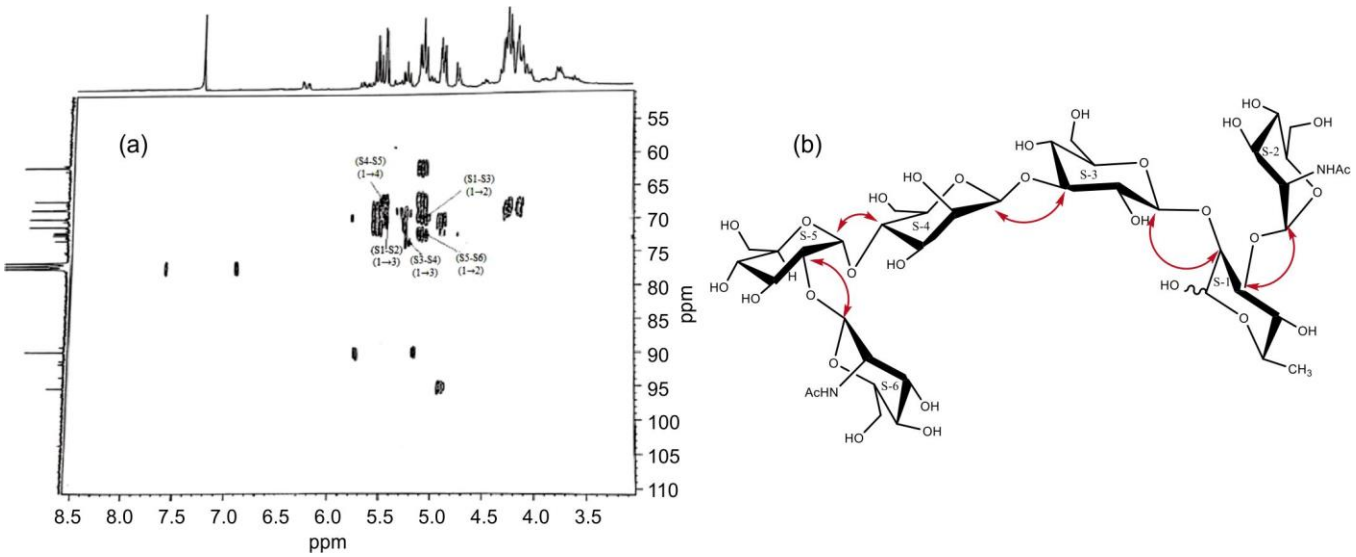

Fig. 4. (a) HMBC spectrum of magnorhamnose acetate in $CDCl_3$ at 300 MHz and (b) HMBC connectivity in magnorhamnose

peaks at δ 4.90×5.30, δ 4.90×3.64 and δ 4.90×4.48 which were confirmed as H-2, H-3 and H-4, respectively by COSY spectrum of magnorhamnose acetate. The chemical shift at δ 3.64 assigned to H-3 of S3 showed that it was glycosidically available for the next monosaccharide unit. Further the chemical shift of δ 3.64 ppm does not give any cross peak in its HMBC spectrum therefore it discontinued the linkage process and it was confirmed as disaccharide. It was examined in the HSQC spectrum which gave a cross peak δ 3.68×74.0. The chemical shift value of ^{13}C signal at δ 74.0 for H-3 of S-3 which was re-examined in HMBC spectrum resulting a cross peak between δ 74.0×5.20 confirming a (1→3) linkage between S3 and S-4 (reverse HMBC). This anomeric proton value of δ 5.20 gave a cross peak at δ 92.00 in HSQC spectrum of magnorhamnose acetate confirming the anomeric proton/ carbon value as δ 5.2 and 92.0 for S4. The anomeric proton/ carbon value of S-4 at δ 5.20 resemble with the literature value of β-Man*p* that the confirming that S4 was β-Man*p*. The anomeric proton value of S4 (J = 9.0 Hz) confirm the β-glycosidic linkage between S3 and S4. Moreover, it also confirmed a $^4C_1$ D-conformation for S4. The anomeric proton of S4 at δ 5.20 gave three cross peaks at δ 5.20×4.80, δ 5.20×4.50 and δ 5.20×4.19 which were analysed as H-2, H-3 and H-4 of S-4, respectively, by COSY spectrum of compound C. The chemical shift of δ 4.19 was assigned H-4 of S4 reside in the glycosidic linkage region which did not giving any cross peak in HMBC spectrum hence hindering the linkage process therefore it was again observed in the HSQC spectrum, gave a cross peak at δ 67.00 and when it was again observed in HMBC spectrum, it gave a cross peak at δ 67.00×5.60 confirming (1→4) linkage between S4 and S5. This anomeric proton value at δ 5.60 gave a cross peak in HSQC spectrum at δ 93.59 confirming the anomeric proton/carbon value for S5 as δ 5.60×93.59. As these values were comparable with literature value of α-D-Glc*p* confirmed as α-Glc*p*. Further the anomeric proton at δ 5.60 for which J value is < 2 Hz, confirmed α-glycosidic [26] linkage between S4 and S5 and $^4C_1$ L conformation for S5. As we move further the anomeric proton value δ 5.60 gave three cross peaks at δ 5.60×3.72, δ 5.60×5.10 and δ 5.60×4.30 in the TOCSY spectrum of S5 and they confirmed as H-2, H-3 and H-4 of S5. Out of these chemical shifts the value of δ 3.72 assigned H-2 of S-5 was supposed to have the glycosidic linkage with the next monosaccharide linkage, *i.e.* S6. Further, the chemical shift of δ 3.72 did not give any cross peak in HMBC spectrum hence, this linkage was again observed by Reverse HMBC process, getting a cross peak at δ 3.72×72.00 (HSQC). Further, this value of δ 72.00 gave a cross peak at δ 72.00×5.70 in the HMBC spectrum confirming (1→2) linkage between S5 and S6. Further, the anomeric proton value of δ 5.70 gave a cross peak at δ 91.61 confirming the anomeric proton/carbon values of S-6 was at δ 5.70 and 91.61ppm. Since these values resembles with the anomeric proton carbon values of Man*p* and S6 was confirmed β-D-ManNAc in pyranose ring structure. Further the anomeric proton at δ 5.70 (J = 8 Hz) confirm β-glycosidic linkage between S5 and S6 and $^4C_1$ D conformation for S6. Further, the anomeric proton value at δ 5.70 gave three cross peaks at δ 5.70×3.70, δ 5.70 ×5.2 and δ 5.70×5.50 which were confirmed as H-2, H-3 and H-4 of S6, respectively. The chemical shift of H-2, H-3 and H-4 did not exist in the linkage region, confirmed that β-D-Man*p*NAc (S6) was present at non-reducing end of oligosaccharide, which was supported by the COSY spectrum of magnorhamnose acetate in $CDCl_3$ at 300 MHz (Table-1). All the monosaccharide anomeric proton ^1H NMR values *viz*. L-Rha*p*, β-D-Manp, D-ManNAc*p*, α-D-Glc*p* and β-D-Glcp were also confirmed by authentic samples.

The mass spectra of magnorhamnose (Fig. 5) exhibited a characteristic molecular ion peak corresponding to the intact oligosaccharide, along with several daughter ion fragments generated through successive fragmentation pathways. The observed fragmentation pattern confirmed the high molecular weight and oligosaccharide nature of the compound. In addition to the molecular ion signal, the spectrum displayed sodium- and ammonium-associated adduct ions, which are commonly observed in electrospray ionization mass spectrometry of carbohydrate-based compounds. Fragment ions corresponding to monosaccharide units were also detected, further supporting the presence of hexose sugar residues within the structure and the proposed fragmentation pathways are shown in **Scheme-II**.

Thus based on the interpretation of 2D-NMR values and mass spectrum of compound magnorhamnose, the molecular formula was $C_{41}H_{72}N_2O_{30}$ (*m.w.* 1073) and the final structure of novel hexa-saccharide is assigned as below:

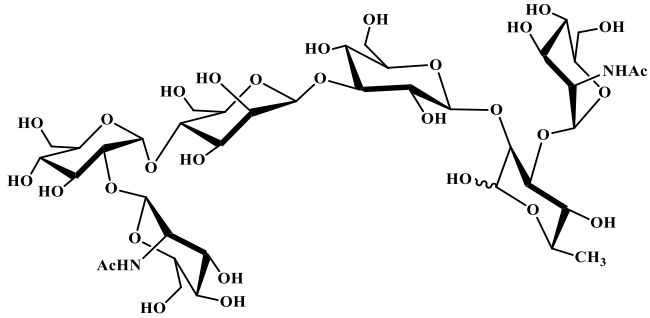

TABLE-1
ASSIGNMENTS OF RING PROTON/CARBON OF MAGNORHAMNOSE ACETATE

Proton	L-Rham*p*	D-ManNHAc*p*	β-D-glc*p*	β-D-man*p*	α-D-glc*p*	β-ManNHAc*p*
H-1	6.25	5.50	4.90	5.20	5.60	5.70
H-2	3.98	4.11	5.30	4.80	3.72	3.70
H-3	4.10	4.28	3.64	4.50	5.10	5.20
H-4	5.28	4.86	4.48	4.19	4.30	5.50

The ^{13}C chemical shifts of the remaining substituents are CH_3O = δ 55.57 ppm; CH_3CON = δ 22.79 ppm; CH_3CON = δ 174.85, 174.90 ppm.

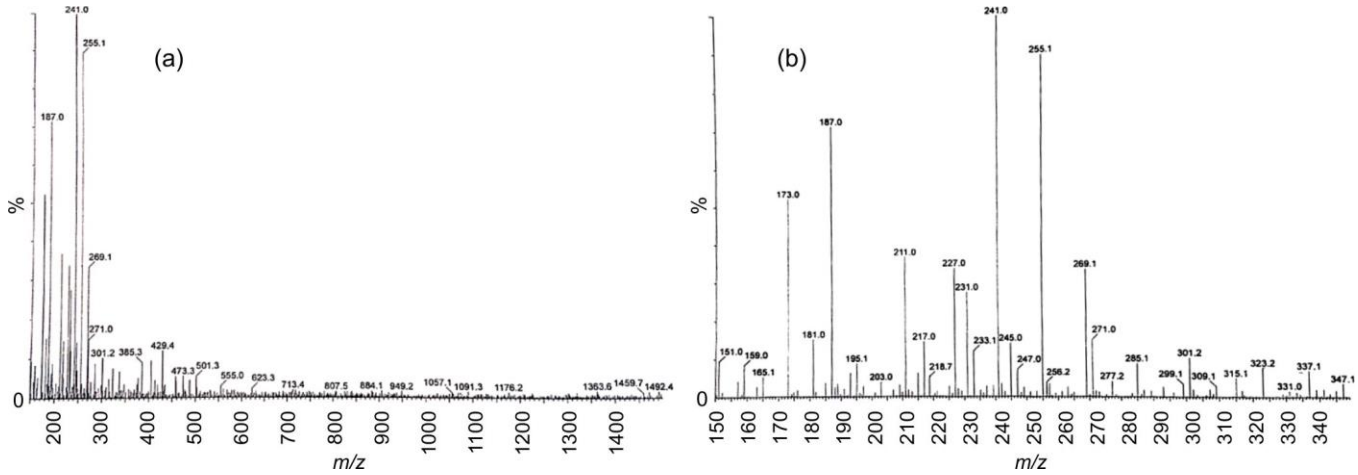

Fig. 5. ESI-mass spectra of magnorhamnose

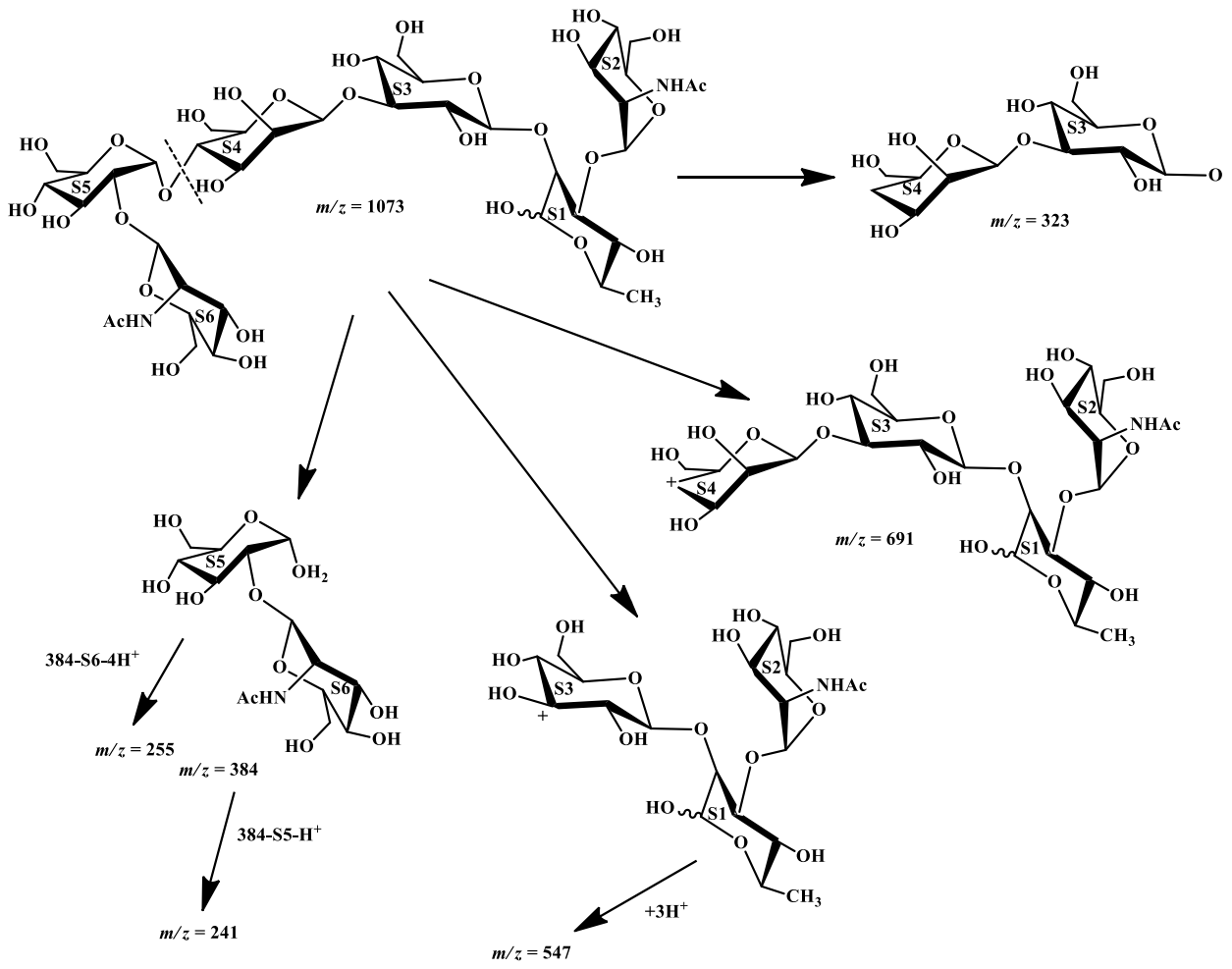

Scheme-II: Mass fragmentation patterns of magnorhamnose

Prediction of biological activities: The PASS server was employed to predict the potential pharmacological activities of the studied compound based on its structural features (https://way2drug.com/). For each predicted activity, the PASS tool provides two probability estimates *viz*. the probability of activity (Pa) and the probability of inactivity (Pi), both ranging from 0.00 to 1.00. These values enable qualitative assessment of the likelihood of specific biological effects associated with the compound. The selected compound was analysed using the PASS server to gain deeper insight into its prospective pharmacological profile and the predicted activities are summarised in Table-2.

Molecular docking results

Wound healing mechanism: To explore the possible involvement of compound C in wound-healing pathways, mole-

TABLE-2
PREDICTION OF THE BIOLOGICAL ACTIVITIES OF ISOLATED COMPOUND C *via* PASS

Biological activity	Pa value
Antibacterial	0.751
Antifungal	0.740
Antibiotic	0.606
Wound healing agent	0.590
Antioxidant	0.512
Anti-inflammatory	0.498

cular docking studies were carried out against five target proteins associated with tissue repair and cellular regeneration, namely 1FLT, 1Q7D, 2AZ5, 6Y8M and 6B8Y. The docking analysis demonstrated favourable ligand–protein interactions, with binding energies indicating appreciable affinity of compound C toward these wound-healing-related targets. The mechanism of wound healing is depicted in Fig. 6 and the molecular docking data given in Table-3.

Among the studied proteins, the strongest interaction was observed with protein 1FLT, followed by 2AZ5, sugges-

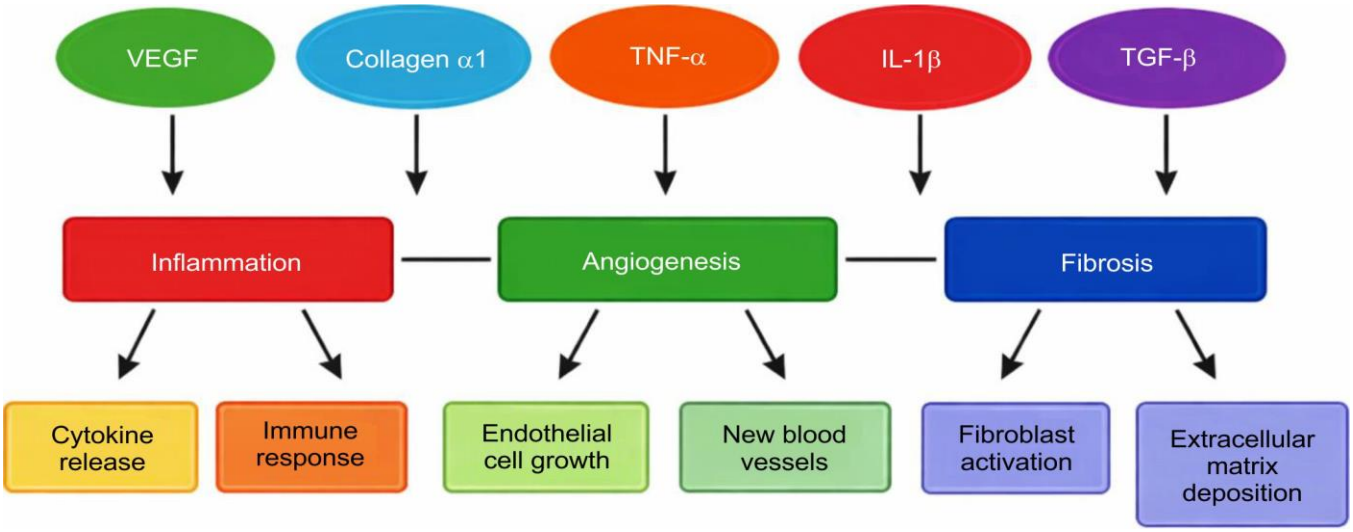

Fig. 6. The plausible mechanism of wound healing

TABLE-3
MOLECULAR DOCKING BINDING ENERGY VALUES AND PROTEIN-LIGAND INTERACTIONS

PDB ID	Binding energy (kcal/mol)	2D structure of protein-ligand	3D structure of protein-ligand
1FLT	-8.0	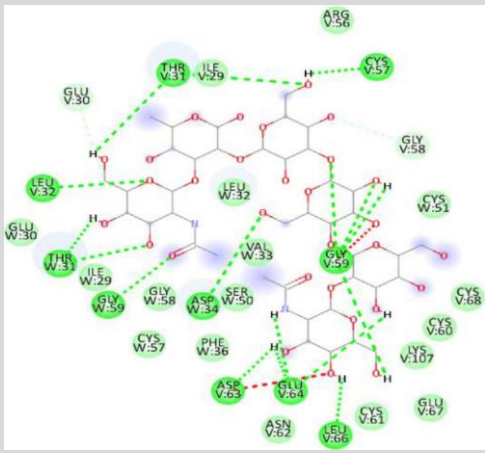	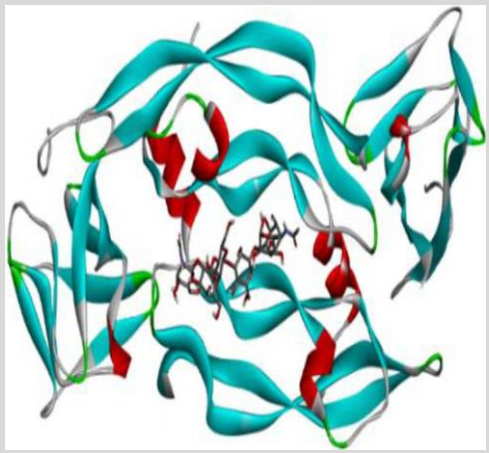
1Q7D	-5.2	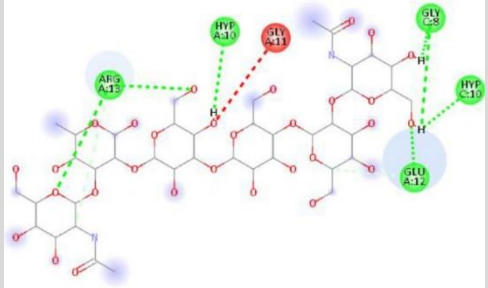	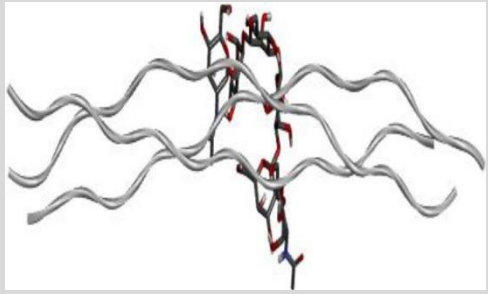

2AZ5	-7.5	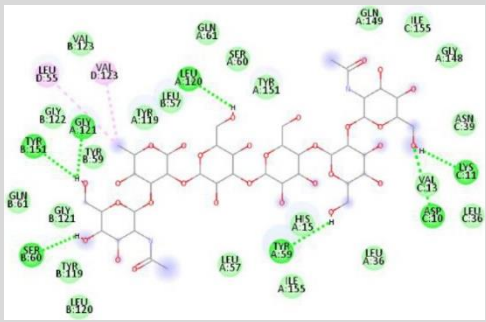	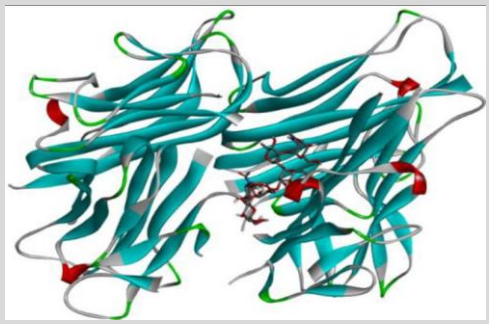
6Y8M	-5.6	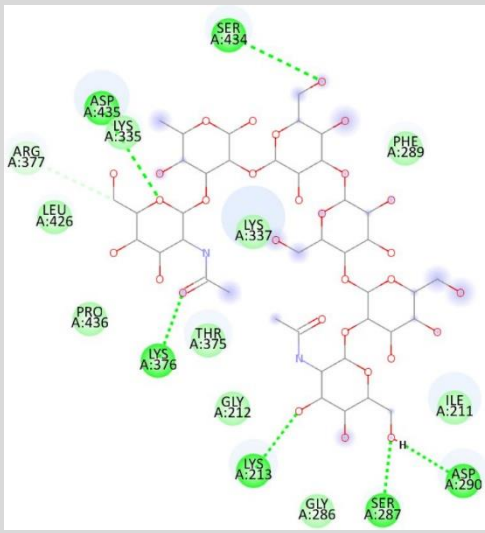	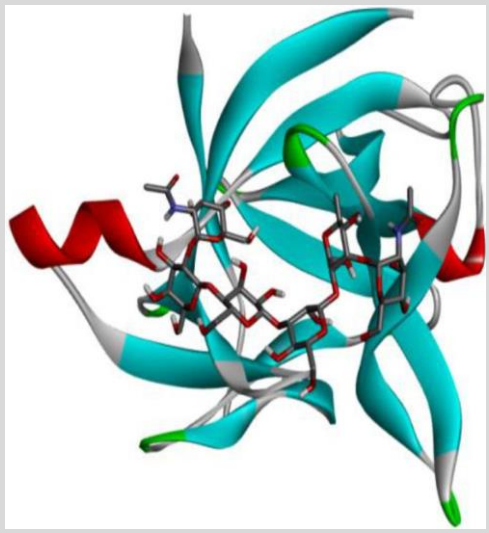
6B8Y	-5.6	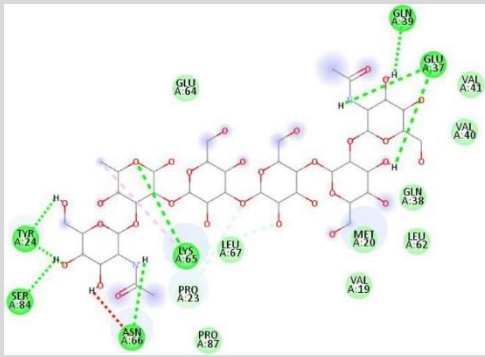	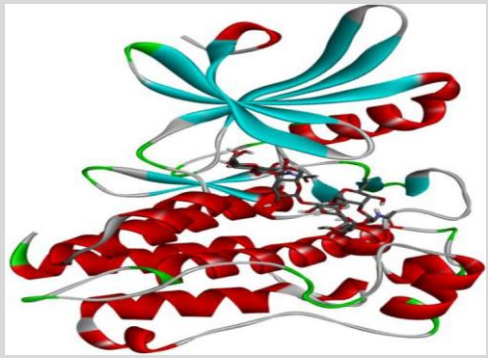

ting a potential role of the compound in modulating pathways associated with angiogenesis, cell proliferation and tissue regeneration. The observed molecular interactions correlate well with the structural features of the oligosaccharide and support its possible therapeutic relevance in wound-healing applications. These findings provide a computational basis for further biological and pharmacological investigations of compound C as a potential natural wound-healing agent.

Vascular endothelial growth factor (VEGF) (PDB code: 1FLT): The docking pose shown in Fig. 7 demonstrates that the rhamnose-containing hexasaccharide is well accommodated within the active binding pocket of the target protein, where it forms multiple stabilizing hydrogen-bond interactions with surrounding amino acid residues. The ligand interacts with several important residues including Asp34, Thr31, Lys31, Gly59, Leu32, Leu66, Glu64, Cys57, Gly58, and Gly5, contributing to the stabilization of the ligand–

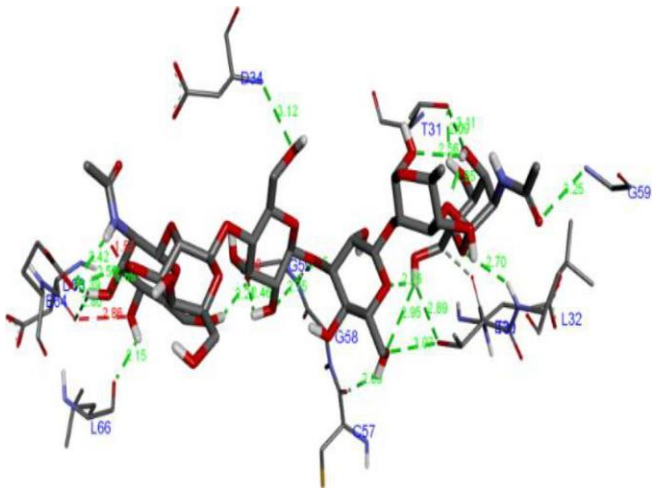

Fig. 7. Docking pose of VEGF (PDB: 1FLT) with ligand

protein complex. At the left region of the binding pocket, Glu64 and Leu66 interact with the hydroxyl groups of the oligosaccharide through hydrogen bonds with bond distances ranging from ~2.15 to 2.86 Å, providing strong anchoring of the ligand within the active site. The abundant hydroxyl groups present in the carbohydrate framework actively participate in these polar interactions, thereby enhancing binding stability. Within the central region of the binding cavity, residues Gly5, Gly58 and Cys57 establish additional hydrogen-bond interactions with bond distances of approximately ~2.04-2.95 Å. These interactions help maintain the appropriate orientation and conformational stability of the oligosaccharide backbone inside the binding pocket through a combination of H-bonding and van der Waals interactions.

On the right side of binding site, Thr31, Lys31, Gly59 and Leu32 form further hydrogen-bond interactions with the terminal sugar units of the hexasaccharide, exhibiting bond distances in the range of ~2.25-2.70 Å. These interactions support the ligand–protein interaction network and contribute to the stable accommodation of the oligosaccharide within the active site. Further, the observed hydrogen-bond distances within the range of ~2.0-3.1 Å indicate strong and favourable ligand–protein interactions. The extensive hydrogen-bonding network and stable binding orientation support the docking results and suggest the potential biological relevance of the rhamnose-containing hexasaccharide in wound-healing applications.

Collagen α-1 (PDB code: 1Q7D): The docking conformation presented in Fig. 8 demonstrates that the rhamnose-containing hexasaccharide binds effectively within the active site of collagen α-1 through multiple hydrogen-bond and polar interactions. The ligand is stabilized by several key amino acid residues including Gly8, Gly11, Lys10, and Arg13, which together surround the binding cavity and contribute to the stability of the ligand–protein complex. Residue Gly8 forms hydrogen-bond interactions with the hydroxyl groups of the oligosaccharide at an approximate bond distance of 2.06 Å indicating strong ligand–protein association. Similarly, Gly11 participates in multiple hydrogen-bond interactions with bond distances ranging from approximately 1.94 to 1.97 Å, suggesting highly favourable interactions within the active site. These interactions play an important role in maintaining the proper orientation and stabilization of the oligosaccharide within the binding pocket.

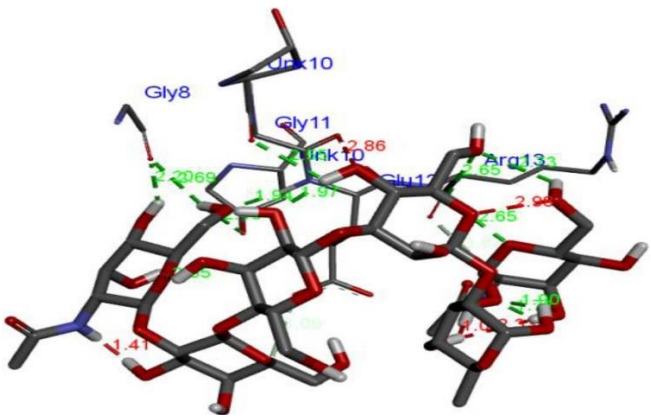

Fig. 8. Docking pose of collagen α-1 (PDB: 1Q7D) with ligand

Moreover, Lys10 forms hydrogen-bond interactions with the ligand at a distance of approximately 2.86 Å, contributing to effective anchoring of the oligosaccharide inside the active site. The positively charged residue Arg13 further enhances ligand stabilization through hydrogen-bond interactions with bond distances of approximately 2.65 Å. Several additional hydrogen bonds are also observed between the hydroxyl groups of the hexasaccharide and neighbouring amino acid residues, with interaction distances generally ranging from ~1.9 to 2.9 Å. These short bond distances indicate strong and favourable ligand–protein interactions. Thus, the extensive hydrogen-bonding network suggests a stable binding conformation of the rhamnose-containing hexasaccharide with collagen α-1, supporting its possible role in wound-healing and tissue-regeneration processes.

Tumar necrosis TNF-α (PDB code: 2AZ5): The docking pose, shown in Fig. 9, demonstrates that the rhamnose-containing hexasaccharide binds effectively within the active site cavity of TNF-α through multiple hydrogen-bond and polar interactions. The ligand interacts with key amino acid residues including Asp10, Lys11, Leu55, Tyr59, Ser60, Leu120, Gly121 and Val123, stabilize the ligand–protein complex.

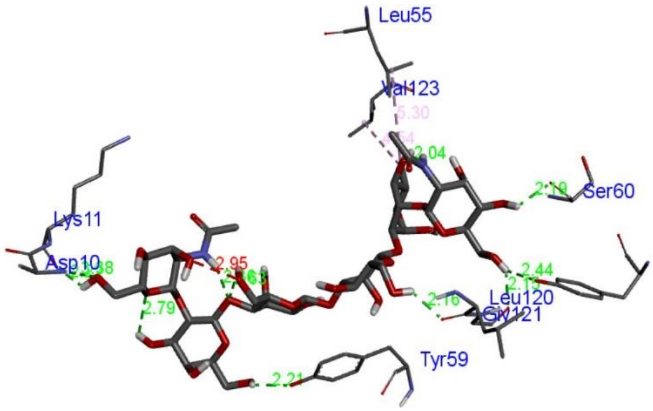

Fig. 9. Docking pose of TNF-α (PDB: 2AZ5) with ligand

At the left region of the binding pocket, Asp10 forms hydrogen-bond interactions with the hydroxyl groups of the oligosaccharide at bond distances of ~2.7-2.9 Å, contributing to stable anchoring of the ligand within the active site. Lys11 further supports ligand stabilization through electrostatic and polar interactions. In the central region of binding cavity, Tyr59 and Ser60 establish strong hydrogen-bond interactions with bond distances of ~2.19-2.21 Å, which help in maintaining the proper orientation of the carbohydrate moiety within the binding pocket. Residues Leu120 and Gly121 also participate in ligand stabilization through hydrogen-bond and van der Waals interactions, with distances ranging from ~2.16 to 2.44 Å. Furthermore, Val123 also forms a hydrophobic interaction with the ligand at an approximate distance of 5.30 Å, while Leu55 contributes to hydrophobic stabilisation within the binding cavity. The observed hydrogen-bond distances of ~2.1-2.9 Å also indicate favourable and stable ligand–protein interactions. The multiple hydroxyl groups present in the hexasaccharide facilitate extensive hydrogen bonding with active-site residues, thereby enhancing the binding stability of the complex.

Interleukin-1β (PDB code: 6Y8M): The molecular docking study revealed that the isolated rhamnose-containing hexasaccharide also interacts strongly with the active-site residues of interleukin-1β through multiple hydrogen bonding and polar interactions. As shown in Fig. 10, the ligand forms stabilizing interactions with key amino acid residues including Glu3, Gln, Lys65, Asn66, Ser84, Pro23 and Tyr24. Hydrogen-bond interactions were observed with bond distances ranging from ~2.16 to 3.31 Å, indicating favourable and stable ligand–protein binding. Whereas residues Glu3 and Gln participate in hydrogen bonding with bond distances of approximately 2.8 Å and 2.35 Å, respectively, contributing to effective anchoring of the ligand within the binding pocket. Lys65 and Asn66 also form hydrogen-bond interactions at the distances of ~3.31 Å and 2.38 Å, respectively, further stabilizing the orientation of the oligosaccharide inside the active site. Further interactions involving Ser84, Pro23 and Tyr24, with bond distances ranging from ~2.19 to 2.99 Å, help to maintain the ligand within the binding cavity through additional hydrogen-bond and polar interactions.

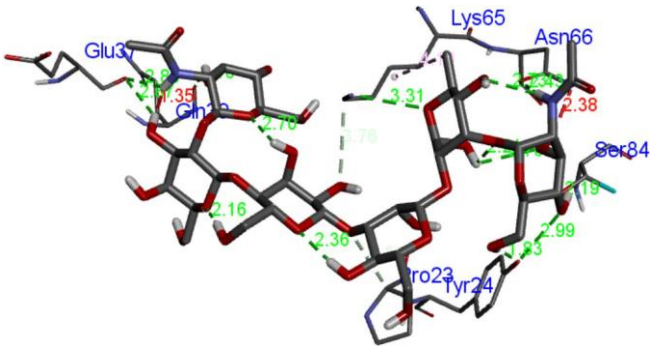

Fig. 10. Docking pose of interleukin-1β (PDB: 6Y8M) with ligand

Transforming growth factor-β (TGF-β, PDB code: 6B8Y): The docking pose shown in Fig. 11 demonstrates that the rhamnose-containing hexasaccharide binds effectively within the active site of TGF-β through multiple hydrogen-bond and polar interactions. The ligand establishes multiple stabilizing interactions with the key active-site residues including Asp290, Ser287, Lys213, Ser434, Asp435, Arg377 and Lys376, thereby contributing to the strong stabilization and favorable binding affinity of the ligand–protein complex. Ser287 forms strong hydrogen-bond interactions with the hydroxyl groups of the oligosaccharide at bond distances of ~2.45-2.56 Å, contributing to stable anchoring of the ligand within the binding pocket. Asp290 also participates in ligand stabilization through hydrogen-bond interactions with adjacent hydroxyl groups.

Additional stabilization of the ligand within the binding cavity is provided by Ser434 and Asp435, which form H-bond interactions at distances of ~2.47 Å and 2.52 Å, respectively. These interactions assist in maintaining an energetically favourable orientation of the hexasaccharide inside the active site. Lys376 further reinforces the binding through a H-bond at ~2.34 Å, whereas Arg377 contributes *via* polar contacts that support the integrity of the docking complex. A strong H-bond interaction with Lys213 at ~2.28 Å also plays an important role in strengthening ligand accommodation within

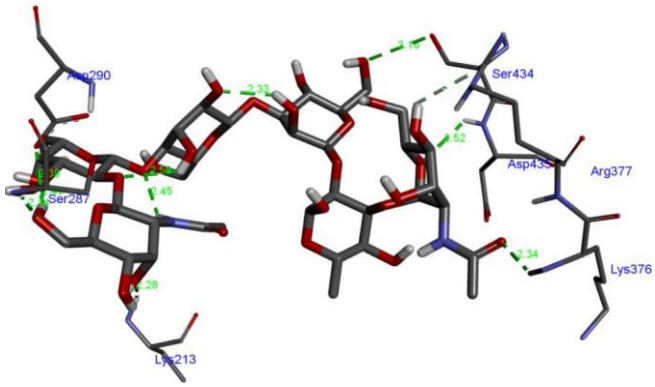

Fig. 11. Docking pose of TGF-β (PDB: 6B8Y) with ligand

the protein cavity. The interaction distances observed throughout the docking complex (~2.28-3.15 Å) fall within the range characteristic of stable hydrogen-bond formation, indicating favorable molecular recognition between the ligand and TGF-β. The large number of hydroxyl groups present in the hexasaccharide enables the formation of an extensive interaction network, thereby enhancing binding stability and affinity toward the target protein. Comparative analysis further revealed that the isolated compound exhibited stronger binding affinity than curcumin, which has been reported to show a binding energy of approximately -5.21 kcal/mol against the same protein target [29].

Conclusion

The present study reports the isolation and structural characterization of compound C, a novel hexasaccharide designated as magnorhamnose. The structure was elucidated through detailed interpretation of 1D (^{1}H & ^{13}C) and 2D NMR spectroscopic techniques including HSQC, TOCSY, COSY and HMBC experiments, and was further supported by ESI-mass spectrometric analysis. The finding of magnorhamnose expands the existing repertoire of naturally occurring carbohydrate architectures and highlights the structural diversity and complexity of glycochemistry. To evaluate its possible biological significance, magnorhamnose was subjected to PASS analysis, which provided preliminary insight into its potential pharmacological activities. The predicted bioactivity was further investigated through molecular docking studies against five wound-healing-related protein targets, namely 1FLT, 1Q7D, 2AZ5, 6Y8M, and 6B8Y. The compound exhibited favourable binding affinities with docking energies of -8.0, -5.2, -7.5, -5.6 and -5.6 kcal/mol, respectively, indicating stable ligand–protein interactions. Comparative analysis revealed that curcumin, a well-known bioactive compound, exhibited a binding energy of approximately -5.21 kcal/mol against the same target, which was lower than the binding affinity observed for magnorhamnose. The molecular docking results demonstrated that the multiple hydroxyl groups present in the hexasaccharide facilitate extensive hydrogen-bond and polar interactions within the active sites of the target proteins, thereby contributing to strong binding stability and favourable docking conformations. These results highlight the ligand's potential as a promising lead compound and may represent a promising natural lead compound for future wound-healing and therapeutic investigations.

ACKNOWLEDGEMENTS

The authors are thankful to Head, Department of Chemistry, University of Lucknow, for providing infrastructure and NMR facilities and CDRI (SAIF) (CSIR-New Delhi], Lucknow for mass analysis). Thanks are also due to Prof. Abhinav Kumar, Department of Chemistry, Lucknow University, for their help in NMR analysis.

CONFLICT OF INTEREST

The authors declare that there is no conflict of interests regarding the publication of this article.

DECLARATION OF AI-ASSISTED TECHNOLOGIES

During the preparation of this manuscript, the authors used an AI-assisted tool(s) to improve the language. The authors reviewed and edited the content and take full responsibility for the published work.

REFERENCES

1. J.M. Da Costa Leite, L.S. Trugo, L.S.M. Costa, L.M.C. Quinteiro, O.M. Barth, V.M.L. Dutra and C.A.B. Maria, *Food Chem.*, **70**, 93 (2000); https://doi.org/10.1016/S0956-7135(99)00115-2
2. E. Schievano, M. Tonoli and F. Rastrelli, *Anal. Chem.*, **89**, 13405 (2017); https://doi.org/10.1021/acs.analchem.7b03656
3. M.M. Rahman, M.N. Alam, N. Fatima, H.M. Shahjalal, S.H. Gan and M.I. Khalil, *J. Food Biochem.*, **41**, e12405 (2017); https://doi.org/10.1111/jfbc.12405.
4. J. Majtan, *Wound Repair Regen.*, **22**, 187 (2014); https://doi.org/10.1111/wrr.12117
5. Z. Li, Q. Huang, Y. Zheng, Y. Zhang, B. Liu, W. Shi and Z. Zeng, *Nutrients*, **15**, 435 (2023); https://doi.org/10.3390/nu15020435
6. N. Kapoor and R. Yadav, *Natl. J. Maxillofac. Surg.*, **12**, 233 (2021); https://doi.org/10.4103/njms.NJMS_154_20
7. Z. Li, Q. Huang, Y. Zheng, Y. Zhang, B. Liu, W. Shi and Z. Zeng, *Nutrients*, **15**, 435 (2023); https://doi.org/10.3390/nu15020435
8. S. Oelschlaegel, M. Gruner, P.-N. Wang, A. Boettcher, I. Koelling-Speer and K. Speer, *J. Agric. Food Chem.*, **60**, 7229 (2012); https://doi.org/10.1021/jf300888q
9. Y. Li, J. Yao, C. Han, J. Yang, M.T. Chaudhry, S. Wang, H. Liku and Y. Yin, *Nutrients*, **8**, 167 (2016); https://doi.org/10.3390/nu8030167
10. P. Truchado, F. Ferreres, L. Bortolotti, A.G. Sabatini and F.A. Tomas-Barberan, *J. Agric. Food Chem.*, **56**, 8815 (2008); https://doi.org/10.1021/jf801625t
11. D.S. Lee, S. Sinno and A. Khachemoune, *Am. J. Clin. Dermatol.*, **12**, 181 (2011); https://doi.org/10.2165/11538930-000000000-00000
12. S.K. Saikaly and A. Khachemoune, *Am. J. Clin. Dermatol.*, **18**, 237 (2017); https://doi.org/10.1007/s40257-016-0247-8
13. H. Aati, S.Y. Aati, M.A. Khanfar, H.S. Bahr, A.T. Ali, M.E. Rateb, H.M. Hassan and M.A. Darwish, *Chem. Biodivers.*, **22**, e01049 (2025); https://doi.org/10.1002/cbdv.202501049
14. L. Warren, *Nature*, **186**, 237 (1960); https://doi.org/10.1038/186237a0
15. F. Fiegl and V. Anger, Spot Tests in Organic Analysis, Elsevier, edn 7 (1983).
16. R. Huey and G.M. Morris, Using AutoDock 4 with AutoDocktools: A Tutorial, The Scripps Research Institute, USA, pp. 54-56 (2008).
17. A.M. Vijesh, A.M. Isloor, S. Telkar, T. Arulmoli and H.-K. Fun, *Arab. J. Chem.*, **6**, 197 (2013); https://doi.org/10.1016/j.arabjc.2011.10.007
18. O.A. Trott and J. Olson, *J. Comput. Chem.*, **31**, 455 (2010); https://doi.org/10.1002/jcc.21334
19. W.L. DeLano, Pymol: An Open-Source Molecular Graphics Tool, CCP4 Newsletter on Protein Crystallography, vol. 40, pp. 82-92 (2002).
20. X.L. Ouyang, T.H. Ma, G.-L. Xie, S. Chen, H.-S. Wang, Q. Jia, E.-D. Zhang and J.-H. Huang, *Chem. Biodivers.*, **18**, e2100272 (2021); https://doi.org/10.1002/cbdv.202100272
21. J. Gao, G. Shi, G. Song, Y. Shao and B. Zhou, *Magn. Reson. Chem.*, **34**, 249 (1996); https://doi.org/10.1002/(SICI)1097-458X(199604)34:4<249::AID-OMR877>3.0.CO; 2-O
22. S. Bala, N. Mishra, S. Modanwal, A. Yadav and D. Deepak, *Trends Carbohydr. Res.*, **17**, 60 (2025).
23. H. Killiani, *Sugars IX*, **63B**, 369 (1930).
24. C.M. Courtin, H. Van den Broeck and J.A. Delcour, *J. Chromatogr. A*, **866**, 97 (2000); https://doi.org/10.1016/S0021-9673(99)01064-X
25. M. Sharma, M. Shukla and D. Deepak, *Trends Carbohydr. Res.*, **16**, 56 (2024).
26. C.A. Bush, *Bull. Magnet. Resonance*, **10**, 73 (1988).
27. M. Lolli, D. Bertelli, M. Plessi, A.G. Sabatini and C. Restani, *J. Agric. Food Chem.*, **56**, 1298 (2008); https://doi.org/10.1021/jf072763c
28. M.U. Roslund, E. Säwén, J. Landström, J. Rönnols, K.H.M. Jonsson, M. Lundborg, M.V. Svensson and G. Widmalm, *Carbohydr. Res.*, **346**, 1311 (2011); https://doi.org/10.1016/j.carres.2011.04.033
29. G. Sabarees, V. Velmurugan and V.R. Solomon, *Chem. Phys. Impact*, **8**, 100441 (2024); https://doi.org/10.1016/j.chphi.2023.100441